Analytica Chimica Acta 669 (2010) 68–74

Contents lists available at ScienceDirect

Analytica Chimica Acta

journal homepage: www.elsevier.com/locate/aca

A urea biosensor based on pH-sensitive Sm_2TiO_5 electrolyte–insulator–semiconductor

Tung-Ming Pan[a,*], Ming-De Huang[a], Wan-Ying Lin[b], Min-Hsien Wu[c]

[a] Department of Electronics Engineering, Chang Gung University, 259 Wen-Hwa 1st Road, Kwei-Shan, Taoyuan 333, Taiwan, ROC
[b] School of Medicine, Chang Gung University, Taoyuan 333, Taiwan, ROC
[c] Graduate Institute of Biochemical and Biomedical Engineering, Chang Gung University, Taoyuan 333, Taiwan, ROC

ARTICLE INFO

Article history:
Received 18 February 2010
Received in revised form 22 April 2010
Accepted 23 April 2010
Available online 13 May 2010

Keywords:
Urea
Biosensor
pH-sensitive
Sm_2TiO_5
Electrolyte–insulator–semiconductor

ABSTRACT

A urea biosensor based on pH-sensitive Sm_2TiO_5 electrolyte–insulator–semiconductor (EIS) has been described. We used X-ray diffraction, Auger electron spectroscopy, and atomic force microscopy to investigate the structural and morphological features of high-*k* Sm_2TiO_5 sensing membranes that had been subjected to annealing at different temperatures. The EIS device incorporating a high-*k* Sm_2TiO_5 sensing film that had been annealed at 900 °C exhibited good sensing characteristics, including a high sensitivity of 60.5 mV/pH (in solutions from pH 2 to 12), a small hysteresis voltage of 2.72 mV (in the pH loop $7 \rightarrow 4 \rightarrow 7 \rightarrow 10 \rightarrow 7$), and a low drift rate of 1.15 mV h^{-1} (in the buffer solution at pH 7). The Sm_2TiO_5 EIS device also showed a high selective response towards H^+. This improvement can be attributed to the small number of crystal defects and the large surface roughness. In addition, the urea biosensor based on pH-sensitive EIS incorporating a Sm_2TiO_5 sensing membrane annealed at 900 °C allowed the potentiometric analysis of urea, at concentrations ranging from 0.1 to 32 mM, with a sensitivity of 72.85 mV/purea.

1. Introduction

Ion-selective field-effect transistors (ISFETs) were first developed by Bergveld in the 1970s [1] as an alternative to the fragile glass electrode for the measurement of pH and concentrations of ions (Cl^-, Na^+, K^+, NH_4^+, Ca^{2+}, etc.). ISFETs are playing an important role in the development of chemical sensors and biosensor because of the small size of their sensitive area, robustness, high sensitivity, low output impedance, rapid response, low sample volumes, batch processing capability, and the potential for on-chip circuit integration [2]. Many different types of insulator materials, such as Al_2O_3, Si_3N_4, Ta_2O_5, TiO_2, SnO_2, and WO_3 [3–7], can be used for obtaining a pH response. These materials have some disadvantages, however, such as hysteresis and drift effects, which lower the accuracy of their resulting sensors. To extend the application of pH-ISFET sensors, it will be necessary to develop insulator materials that possess high pH sensitivity, small hysteresis, high stability, and low drift. High-dielectric-constant (high-*k*) materials, including ZrO_2, HfO_2, Y_2O_3, Pr_2O_3, Gd_2O_3, and Er_2O_3 [8–13], have recently been proposed as pH-sensitive membranes due to their good sensing performance in electrolyte–insulator–semiconductor (EIS) devices. To improve the quality of the interface between the high-*k* material and the silicon substrate, growing a thin SiO_2 film on the Si substrate imparts the pH sensing membrane with a smaller density of the interfacial state, lower stress, and good adhesion [14].

In recent years, the samarium oxide (Sm_2O_3) films have been considered as potential gate insulators because of their reasonably high relative permittivity (15–30), good thermal stability, and large conduction band offset (>2 eV) [15]. We have previously reported that a Sm_2O_3 gate dielectric exhibited excellent electrical characteristics such as a small equivalent oxide thickness, low gate leakage current, and small frequency dispersion [16]. In addition, the incorporation of TiO_2 or Ti into the lanthanide oxide dielectrics has attracted a considerable amount of attention as a method to achieve a high-*k* gate oxide material with excellent physical and electrical properties for complementary metal-oxide-semiconductor (CMOS) applications [17,18]. Jeon and Hwang showed that a $PrTi_xO_y$ film deposited on the Si substrate by physical vapor deposition (PVD) exhibited a lower reactivity to water, thinner interfacial layer, higher capacitance value and lower leakage current [19]. In this paper, the physical properties and sensing characteristics of thin Sm_2TiO_5 films deposited on a Si substrate by means of reactive co-sputtering were studied. In addition, we determined the effect that postdeposition annealing (PDA) treatment had on the sensing characteristics (pH sensitivity, hysteresis, drift, and selectivity) of these films. Furthermore, as a demonstration case for urea biosensor based on pH-sensitive Sm_2TiO_5 EIS, urease-immobilized film was prepared by the entrapment of enzyme molecules in alginate hydrogel.

* Corresponding author. Tel.: +886 3 211 8800x3349; fax: +886 3 211 8507.
E-mail address: tmpan@mail.cgu.edu.tw (T.-M. Pan).

0003-2670/$ – see front matter © 2010 Elsevier B.V. All rights reserved.
doi:10.1016/j.aca.2010.04.045

2. Experimental

2.1. Reagents and materials

Silicon wafers were used as the substrate for the Sm_2TiO_5 sensing membrane. The silicon substrate was (1 0 0)-oriented p-type with resistivity 1–10 Ω cm. Thin Sm_2TiO_5 film was deposited onto the silicon substrate maintained at 25 °C using radio frequency co-sputtering from a 3 in.-diameter, 1/4 in.-thickness, and 99.95% purity samarium target and titanium metal target. During deposition the total pressure was maintained at $\sim 10^{-3}$ Torr. A urease activity of $\sim 100\ U\ mg^{-1}$ was obtained from Jack Beans; unless otherwise stated, all chemicals were purchased from Sigma.

2.2. Preparation of pH-EIS sensor

Before deposition of the Sm_2TiO_5 film, the wafers were cleaned using a standard RCA process and then they were treated with 1% HF to remove the native oxide. A ~40 nm Sm_2TiO_5 film was deposited on the Si substrate through reactive co-sputtering from a samarium target and a titanium target in diluted O_2. Subsequently, samples were annealed in O_2 ambient for 30 s by rapid thermal annealing (RTA) at various temperatures to form Sm_2TiO_5. The backside contact (a 400-nm-thick Al film) of the Si wafer was deposited using a thermal coater. The sensing membrane size was defined through photolithographic processing under a photosensitive epoxy (SU8-2005, MicroChem) that behaved as an anti-acid polymer. EIS devices were then fabricated on the Cu lines of a printed circuit board by using a Ag gel to form conductive lines. A handmade epoxy package was employed to encapsulate the EIS structure and the Cu line.

2.3. Evaluation of the structural and sensing properties of pH-EIS device

The thickness of Sm_2TiO_5 thin films was determined using spectroscopic ellipsometry. The film structure and composition of the Sm_2TiO_5 sensing films after PDA at various temperatures were investigated through use of a combination of X-ray diffraction (XRD) and Auger electron spectroscopy (AES). The surface morphologies of the Sm_2TiO_5 films were checked by atomic force microscopy (AFM). The pH sensitivities of the Sm_2TiO_5 sensing membranes were determined by capacitance–voltage (C–V) curves of EIS devices. The C–V curves in different pH buffer solutions (Merck Inc.) were measured through Hewlett-Packard 4284A LCR meter operated at an ac signal frequency of 100 Hz. A Ag/AgCl reference electrode (commercial liquid-junction electrode) was connected with sense line and a EIS device copper line was connected with force line. All setups were protected in dark box to avoid light and noise interference.

2.4. Fabrication of EIS-based urea biosensor

A urease solution prepared in phosphate-buffered saline (PBS) was thoroughly mixed with an alginate suspension to form a urease/alginate suspension having concentrations of $0.1\ mg\ L^{-1}$ and 1.5% (w/v), respectively. The suspension was loaded onto a clean glass slide and then covered with another glass slide, leaving a 1-mm-thick spacer in between to define the thickness of the alginate thin layer. In the subsequent gelatinization process, the sandwich-like structure was submerged in 102 mM $CaCl_2$ for ~10 min. A thin urease-containing alginate gel was subsequently shaped according to the zone of the Sm_2TiO_5 sensing membrane using a borer; it was then attached to the surface of the sensing membrane. Urea solutions having concentrations of 0.01, 0.05, 0.1, 0.5, 1, 2, 4, 8, 16, 32, 128, and 300 mM were prepared from urea powder and PBS; the pH in each solution was measured using a commercial pH meter.

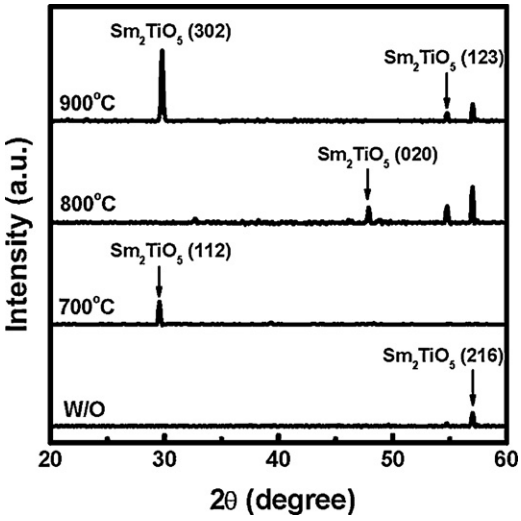

Fig. 1. XRD analysis of Sm_2TiO_5 film for as-deposited and annealed samples.

3. Results and discussion

3.1. Structural properties

We used XRD to characterize the crystalline structures of the Sm_2TiO_5 samples before and after PDA treatment (Fig. 1). The significant difference in sharpness, intensity, and orientation of the diffraction peak was observed, implying that the crystal growth and crystallinity of the polycrystalline Sm_2TiO_5 films are strongly affected by the RTA temperature. In the as-deposited sample (without, W/O), only small Sm_2TiO_5 (2 1 6) peak was observed in the XRD pattern, suggesting a crystal nature for this sample. The film annealed at 700 °C exhibited one weak (1 1 2) peak, while the one annealed at 800 °C displayed one strong (2 1 6) peak, and two weak (0 2 0) and (1 2 3) peaks. This finding suggests that the Ti atom cannot obtain enough kinetic energy reaction with Sm_2O_3 to form a better stoichiometry Sm_2TiO_5 structure during PDA temperature less than 800 °C. The intensity of the Sm_2TiO_5 peak increased upon increasing the RTA temperature, indicative of an improved Sm_2TiO_5 structure. On the other hand, a relatively stronger (3 0 2) peak and two weaker (1 2 3) and (2 1 6) peaks appeared in the 2θ plot for the 900 °C annealed sample, indicative of a polycrystalline structure. This suggests a preferential orientation of the crystallites with the (3 0 2) planes of orthorhombic Sm_2TiO_5 parallel to the substrate.

Fig. 2 shows the AES depth profiles of Sm_2TiO_5 film that has been annealed at 900 °C. The sputter time was 640 min. The atomic composition of the film annealed at 900 °C showed a Sm_2TiO_5 compound with a Sm:Ti:O ratio of approximation 24:12:64. It is found that a small amount of silicate layer ($SmSi_xO_y$) forms at the interface between the dielectric film and the Si substrate. For silicate formation in the film, the reaction progressed by diffusion of Si from the substrate to the dielectric layer [16].

Fig. 3 displays the AFM surface morphologies of the Sm_2TiO_5 films annealed at different temperatures. The surface roughness of the Sm_2TiO_5 films clearly increased upon increasing the RTA temperature. The Sm_2TiO_5 film performed at 700 °C possessed a smooth surface (0.518 nm), whereas the one annealed at 900 °C showed a rough surface (2.632 nm). We suggest that this behavior is due to an increased self-diffusion of samarium, titanium and oxygen during high-temperature annealing leading to the enhancement of the clustering of grains, thus increasing the sur-

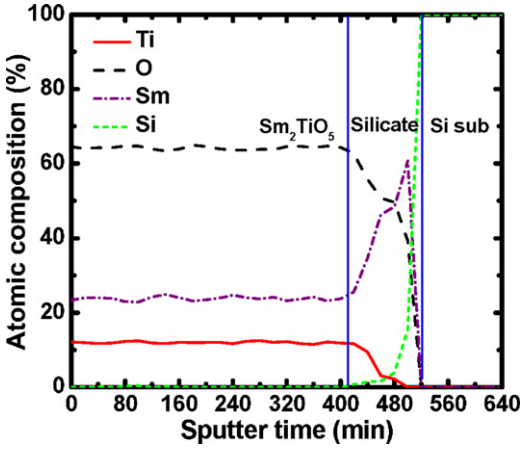

Fig. 2. AES depth profiles of Sm_2TiO_5 film annealed at 900 °C.

face roughness of the Sm_2TiO_5 film [20]. The surface roughness of Sm_2TiO_5 film annealed at different PDA temperatures reflects on the corresponding the intensity and orientation of the diffraction peak, as shown in Fig. 1.

3.2. Sensing characteristics

The effect of the postdeposition annealing temperature on the pH sensitivity of the Sm_2TiO_5 sensing film can be realized by considering the site-binding model to describe the ionic absorption processes at the electrolyte/oxide interface [21]. The response voltage relies on the surface potential (ψ), which is a function of the membrane material and the pH of the electrolyte. The value of ψ can be obtained from Eq. (1).

$$\psi = 2.303\frac{kT}{q}\frac{\beta}{\beta+1}(\mathrm{pH_{pzc}} - \mathrm{pH}) \quad (1)$$

where k is Boltzmann's constant, T is the temperature of the system, q is the elementary charge, $\mathrm{pH_{pzc}}$ is the pH at the point of zero charge, and β is a parameter that denotes the chemical sensitivity of the gate oxide—it is dependent on the density of surface hydroxyl groups [22]. The $\mathrm{pH_{pzc}}$ of pH-ISFET is given by Eq. (2).

$$\mathrm{pH_{pzc}} = -\log_{10}\left(\frac{K_a}{K_b}\right)^{0.5} \quad (2)$$

where K_a and K_b indicate the equilibrium constants at acid and base point, respectively. Furthermore, the β value is relevant to the chemical sensitivity of gate dielectric and is determined by the density of surface hydroxyl groups, which is given as Eq. (3).

$$\beta = \frac{2q^2N_s\sqrt{K_aK_b}}{kTC_{DL}} \quad (3)$$

where N_s is the total number of surface site per unit area and C_{DL} is the double layer capacitance derived from the Gouy–Chapman–Stern model [23]. Based on the above equations, it can be supposed that the higher N_s (or the higher β) accordingly contributes to a higher sensitivity and also the more linear response of pH detection [11]. Based on the value reported in the literature [22], we assume that the double layer capacitance is 20 $\mu F\,cm^{-2}$ for Sm_2TiO_5 EIS device performed at different RTA temperatures. The values of N_s, K_a, and K_b can be computed from the $\mathrm{pH_{pzc}}$ and β, according to Eqs. (2) and (3). The obtained N_s, K_a, and K_b values are then related to the sensing performance of the Sm_2TiO_5 EIS devices annealed at different PDA temperatures. The results are summarized in Table 1. These values are in good agreement with the literature reported in Ref. [24].

In pH-EIS sensing, the change in the pH of the solution caused a shift in the flatband voltage of the C–V curves. This result is

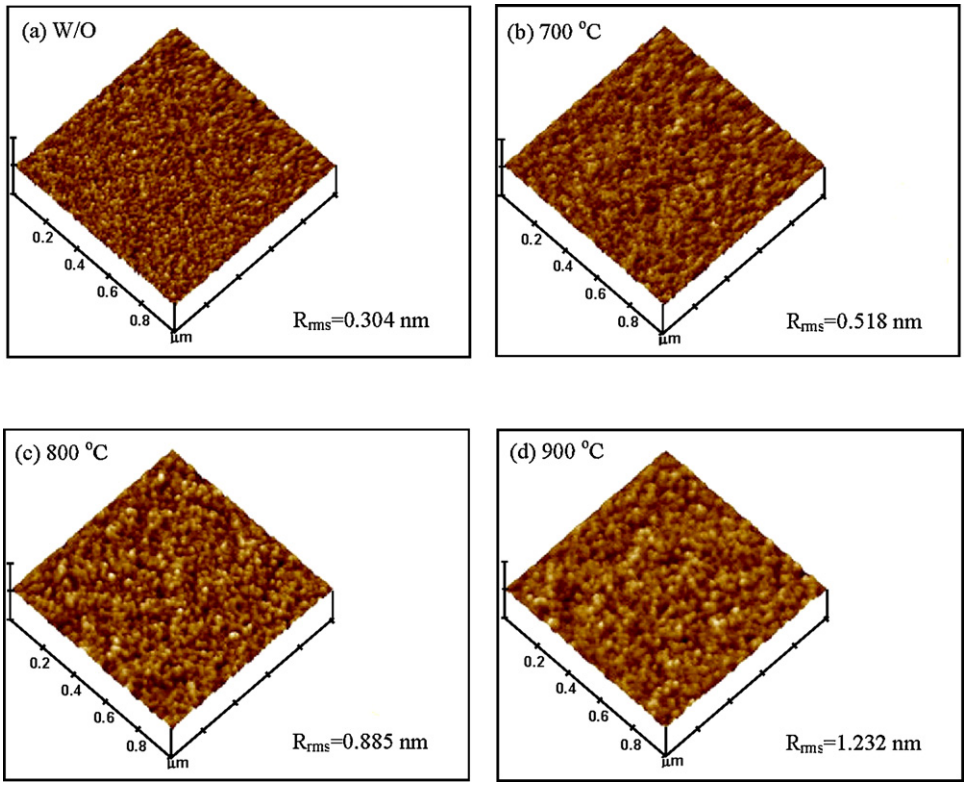

Fig. 3. AFM surface image of Sm_2TiO_5 sensing film for: (a) as-deposited and annealed at (b) 700 °C, (c) 800 °C and (d) 900 °C.

Table 1
The N_s, K_a, and K_b of thin Sm_2TiO_5 sensing membranes after RTA at various temperatures.

RTA temperature (°C)	pH_{pzc}	β	N_s (cm^{-2})	K_a	K_b
W/O	5.66	8.05	4.32×10^{14}	$10^{-7.2}$	$10^{4.1}$
700	5.82	11.84	4.82×10^{14}	$10^{-7.2}$	$10^{4.4}$
800	5.91	27.39	5.58×10^{14}	10^{-7}	$10^{4.8}$
900	6.98	231.1	5.93×10^{14}	$10^{-7.2}$	$10^{6.8}$

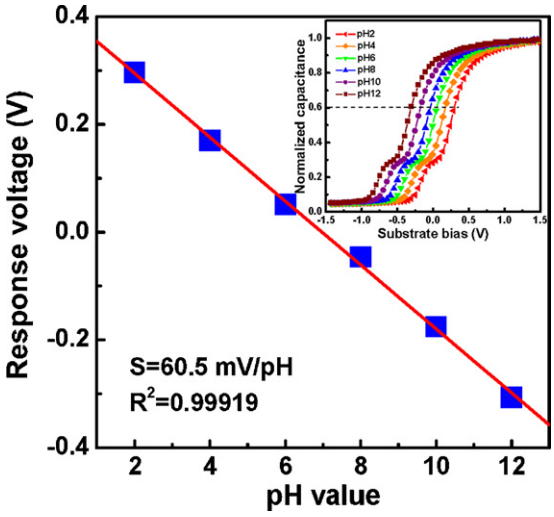

Fig. 4. Response voltage of a Sm_2TiO_5 sensing membrane annealed at 900 °C as a function of pH at room temperature. The inset shows *C–V* curves response of Sm_2TiO_5 dielectrics after PDA at 900 °C when inserted into solutions with pH values from 2 to 12.

mainly due to the ionization of the surface hydroxyl groups by either hydrogen ions or hydroxyl ions. To evaluate the sensing performance of the Sm_2TiO_5 membrane annealed at different temperatures, we recorded a set of *C–V* curves at the pH ranging from pH 2 to 12. Fig. 4 displays the pH-dependence of the response voltage (the voltage required to achieve a normalized capacitance of 0.6) of a Sm_2TiO_5 EIS device that had been subjected to PDA at 900 °C. During a cycle from pH 2 to 12, the response voltage for the Sm_2TiO_5 sensing film annealed at 900 °C shifted by ~605 mV; i.e., the average pH response of this Sm_2TiO_5 film was about 60.5 mV/pH. The inset to Fig. 4 demonstrates the pH-dependence of one group of *C–V* curves for the EIS structure incorporating a Sm_2TiO_5 sensing film annealed at 900 °C. These normalized *C–V* curves were shifted as a result of the change in the number of hydrogen ion on the sensing membrane. It should be noted that the *C–V* curves are deformed in the depletion range, which may be attributed to the presence of interface traps at the interface between silica film and Si substrate. A thin layer of silica formed in the deposition process may produce dense interface traps to affect the behavior of an EIS device [25]. The Sm_2TiO_5 EIS device annealed at 900 °C exhibited a better sensitivity than those of the devices performed at the other RTA temperatures, as shown in Table 2. This result could be attributed to the higher surface roughness of Sm_2TiO_5 sensing membrane at the PDA of 900 °C as observed in the previous AFM analysis. With the higher surface roughness, the N_s will increase accordingly, which therefore contributes to higher detection sensitivity as previously discussed in the site-binding model. In contrast, a low sensitivity could be due to the fact that oxygen atoms diffused from the high-*k* film to the oxide/Si interface during annealing temperature less than 900 °C, causing the formation of Sm-silicate layer [16]. Moreover, the reduction of amorphous silica at the Sm_2TiO_5/Si interface is attributed to the formation of a well-crystallized Sm_2TiO_5 structure at high annealing temperature (900 °C).

Hysteresis phenomenon can be due to the defects of an insulator film, resulting in the formation of porous structures [3]. The interior sites of these porous detects could react with the ions existing in the tested solution and thus causes hysteresis response. Another possible cause is the interaction of ions in the tested solution with the responding sites along the boundaries of grains on an insulator film. We subjected the EIS capacitors prepared under the Sm_2TiO_5 sensing film to pH loops of $7 \rightarrow 4 \rightarrow 7 \rightarrow 10 \rightarrow 7$ and $7 \rightarrow 10 \rightarrow 7 \rightarrow 4 \rightarrow 7$ over a period of 1500 s. The hysteresis voltage here is defined as the gate voltage difference between the initial and terminal voltages measured in the above pH loop. Fig. 5 and Table 2 revealed the profiles and the obtained hysteresis voltages of such evaluation, respectively. Fig. 5 reveals that the hysteresis voltage of the EIS device incorporating a Sm_2TiO_5 sensing film performed at the PDA of 900 °C had hysteresis voltages of 2.72 and 5 mV in the pH loops $7 \rightarrow 4 \rightarrow 7 \rightarrow 10 \rightarrow 7$ and $7 \rightarrow 10 \rightarrow 7 \rightarrow 4 \rightarrow 7$, respectively. It is noteworthy that the acid-side hysteresis was smaller than the base-side hysteresis. The H^+ ions are quickly adsorbed on sensing membrane surface due to the negative surface charge arising from the polarization of Sm_2TiO_5 dielectric [26]. Therefore, the hysteresis in the acid solutions was smaller than that in the alkaline solutions. In addition, a Sm_2TiO_5 EIS device without RTA treatment exhibited a higher hysteresis voltage than those of the devices prepared at the other RTA temperatures, as listed in Table 2. This could be due to a large number of crystal defects in the Sm_2TiO_5.

The drift rate of pH-ISFET is described using a hopping and/or trap-limited transport mechanism, also known as dispersive transport [27,28], to evaluate the hydration rate of the insulator. The phenomena of dispersive transport can be found in a broad class of disordered materials. In an amorphous material, for example, dispersive transport may arise from hopping motion through localized states (hopping transport), trap-limited transport in the presence of traps possessing an exponential energy distribution (multiple-trap transport), or a combination of the aforementioned transport mechanisms (trap-controlled hopping transport) [28]. Dispersive transport causes a decay in the density of sites/traps occupied by the species going through transport [29]. The hypothesis that hydration of the gate dielectric is controlled by a dispersive transport mechanism is sustained by the presence of buried surface sites and/or the presence of traps (specifically electrically active silicon dangling bonds). The variations in the chemical composition of the insulator surface leads to the change in number of surface site with time, thus causing a monotonic temporal increase in the threshold voltage. Fig. 6 shows the drift characteristics of EIS devices incorporating Sm_2TiO_5 sensing membranes annealed at various RTA temperatures, measured in solutions of pH 7 for 12 h. The change in the gate voltage can be defined as $\Delta V_g = V_g(t) - V_g(0)$. The degra-

Table 2
The surface roughness, sensitivity, hysteresis voltage, and drift rate of thin Sm_2TiO_5 sensing membranes after RTA at various temperatures.

RTA temperature (°C)	Surface roughness (nm)	Sensitivity (mV/pH)	Hysteresis voltage (mV)	Drift rate (mV h^{-1})
W/O	0.304	52.95	18	6.52
700	0.518	54.89	15.8	4.77
800	0.885	57.43	14	2.11
900	1.232	60.5	2.72	1.15

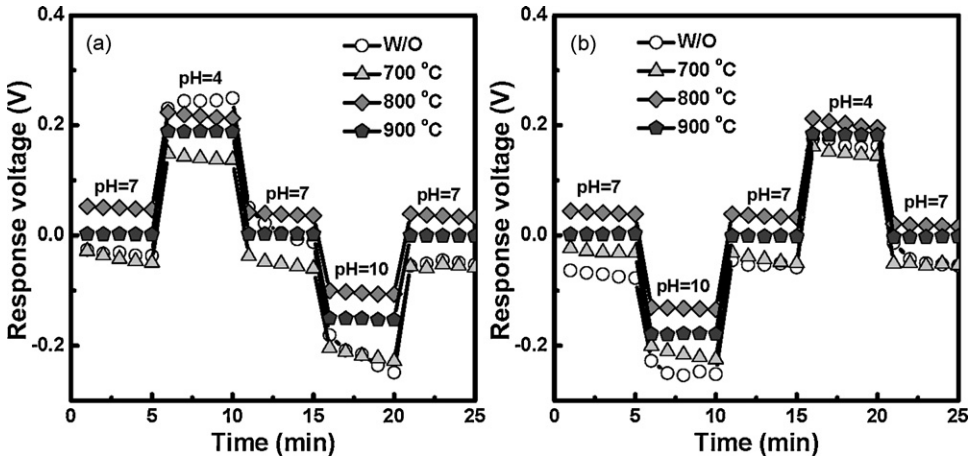

Fig. 5. Hysteresis voltages of EIS devices incorporating Sm_2TiO_5 sensing membranes annealed at various temperatures during the pH loops: (a) 7 → 4 → 7 → 10 → 7 and (b) 7 → 10 → 7 → 4 → 7.

dation slope of the gate voltage variation reflects the EIS stability. The Sm_2TiO_5 EIS capacitor performed at 900 °C exhibited the best long-term stability (slope = 1.15 mV h^{-1}); in contrast, the EIS diode without PDA treatment featured a serious drift of 6.52 mV h^{-1}. The lower drift effect after annealing at 900 °C resulted from the low density of crystal defects. We suspect that higher drift rates is due to a lower surface roughness and a larger number of crystal defects producing the presence of buried surface sites and/or traps.

The selectivity is one of the most important characteristics of an ion sensor, as it often determines whether a reliable measurement in the target sample is possible. Virtually all selectivity considerations based on the Nikolsky–Eisenman equation [30] describe the potentiometric selectivity coefficients, $K^{pot}_{A,B}$ is the potentiometric selectivity coefficient for the primary ion A against the interfering ion B. According to the empirical Nikolsky–Eisenman Eq. (4) as follows:

$$E = E_0 + \frac{RT}{z_A F} \ln\left(a_A + \sum K^{pot}_{A,B} a_B^{Z_A/Z_B}\right) \quad (4)$$

where E is the measured electromotive force (emf); E_0 the constant that includes the standard potential of the electrode, the reference electrode potential, and the junction potential; R the gas constant (8.314 J mol^{-1} K^{-1}); T the absolute temperature in Kelvin; F the Faraday constant (96,490 C mol^{-1}); a_A the activity of primary ion, A; a_B the activity of interfering ion, B; z_A an integer with sign and magnitude corresponding to the charge on the primary ion, A; z_B is an integer with same sign as z_A and magnitude corresponding to the charge on interfering ion, B; and $K^{pot}_{A,B}$ is the potentiometric selectivity coefficient for ion B with respect to the primary ion A.

The selectivity coefficients of potentiometric ion sensors can be determined using different methods [30]. We performed the selectivity coefficients of Sm_2TiO_5 EIS sensors for interfering ion Na^+, K^+, Ca^{2+}, and Mg^{2+} with respect to the primary ion H^+. Separate solution method is used to evaluate the $K^{pot}_{H^+,Na^+}$, $K^{pot}_{H^+,K^+}$, $K^{pot}_{H^+,Ca^{2+}}$, and $K^{pot}_{H^+,Mg^{2+}}$ selectivity coefficients. Fig. 7 displays the response voltage of Sm_2TiO_5 EIS devices annealed at 900 °C vs. various H^+, Na^+, K^+, Ca^{2+}, and Mg^{2+} ion concentrations in pH 7.16. The response curves were measured in the range of H^+, Na^+, K^+, Ca^{2+}, and Mg^{2+} ion concentration from 10^{-5} M to 0.05 M. We obtained selectivity coefficients of Sm_2TiO_5 EIS sensors for ion Na^+, K^+, Ca^{2+}, and Mg^{2+} at −5.94, −5.66, −6.52, and −6.56, respectively. It is evident that the EIS device incorporating a Sm_2TiO_5 sensing membrane has more responsive to H^+ relative to Na^+, K^+, Ca^{2+}, and Mg^{2+}.

The measured as well as extracted sensing parameters are summarized in Table 3, where the data from EIS devices fabricated a Si_3N_4 [31], Al_2O_3 [31], Ta_2O_5 [32], WO_3 [33], HfO_2 [9], Y_2O_3 [10], Pr_2O_3 [11], and $PrTiO_3$ [11] film, are shown for comparison. Although a Sm_2TiO_5 sensing membrane has a slightly higher hys-

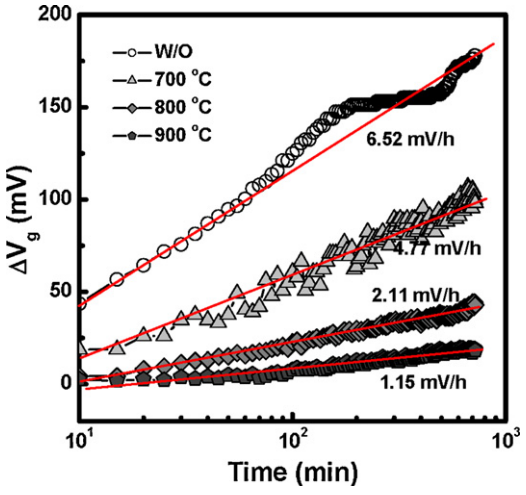

Fig. 6. Drift rates of EIS capacitors incorporating Sm_2TiO_5 sensing membranes after RTA at different temperatures, in a solution at pH 7.

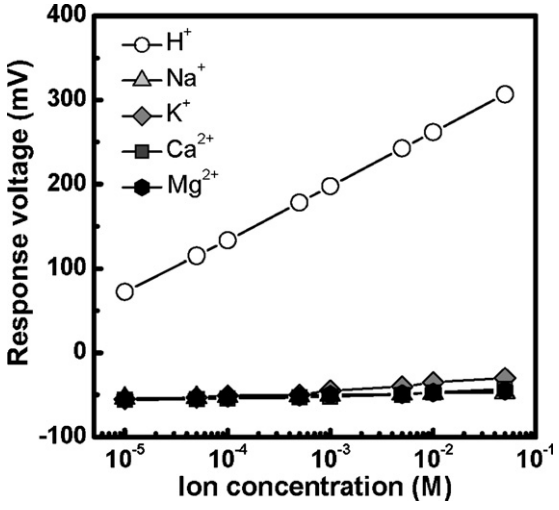

Fig. 7. Response voltage of EIS devices fabricating Sm_2TiO_5 sensing membranes annealed at 900 °C for different H^+, Na^+, K^+, Ca^{2+}, and Mg^{2+} ion concentrations in pH 7.16.

Table 3
Comparison of sensing parameters for EIS device fabricated with a Si_3N_4, Al_2O_3, Ta_2O_5, WO_3, HfO_2, Y_2O_3, Pr_2O_3, $PrTiO_3$, and Sm_2TiO_5.

Sensing membrane	pH sensitivity (mV/pH)	Hysteresis voltage (mV)	Drift rate (mV h^{-1})
Si_3N_4	46–56	3	0.8
Al_2O_3	52–58	0.8	0.3
Ta_2O_5	56–58	<3	<2
WO_3	45–56	15.7	7.2–26
HfO_2	45–58	5–30	2.5–125
Y_2O_3	56.09	13.6	1.24
Pr_2O_3	52.9	17.5	2.15
$PrTiO_3$	56.8	2.84	1.77
Sm_2TiO_5	60.5	2.72	1.15

teresis and drift, the nitrogen incorporated into Sm_2TiO_5 film can reduce the low-*k* silica layer at the Sm_2TiO_5/Si interface and hence improve the sensing characteristics [34].

3.3. Urea biosensor

The detection of urea is of great interest in biomedical and clinical analysis application. An increase of urea concentration in blood and a decreased level of urine are a strong indication of renal dysfunction. The determination of urea is generally performed with enzyme-based biosensors. Therefore a variety of urea biosensors have been developed for the selective determination of many substances using ion-selective membranes in combination with suitable enzymes [35–39]. We prepared a urea biosensor based on pH-sensitive Sm_2TiO_5 EIS device, using urease as the biocomponent. Urease catalyzes the hydrolysis of urea to ammonium, hydroxyl, and bicarbonate ions. The increase in the OH^- ion concentration generates a potential change at the electrode surface that is relative to the urea concentration, in accordance with the reaction

$$NH_2CONH_2 + 3H_2O \xrightarrow{\text{urease}} 2NH_4^+ + OH^- + HCO_3^- \quad (5)$$

For the detection of urea, we used the entrapment method to immobilize the enzyme, using an alginate and $CaCl_2$ solution, which reacted to form calcium alginate, on a Sm_2TiO_5 sensing membrane. This immobilization procedure preserved the native properties of the entrapped enzyme. Fig. 8 presents the shift in the response voltage of the urea biosensor based on pH-sensitive EIS incorporating a Sm_2TiO_5 sensing film (RTA at 900 °C) as a function of the urea concentration. The sensitivity of this biosensor device, in terms of its response to urea concentrations between 0.1 and 32 mM, was 72.85 mV/purea. The stability of the urea biosensor was observed every seven days. After 140 days, the sensitivity of urea biosensor was 72.85 ± 5.6 mV/purea. The sensitivity of urea biosensor was stable. The storage periods of the urea biosensor exceeded four months. Furthermore, the five urea biosensors were used to measure the purea–potential response at the same time for six times. The sensitivity value for the urea biosensor was close to 73 mV/purea. Therefore, we obtained good reproducibility for the urea biosensor.

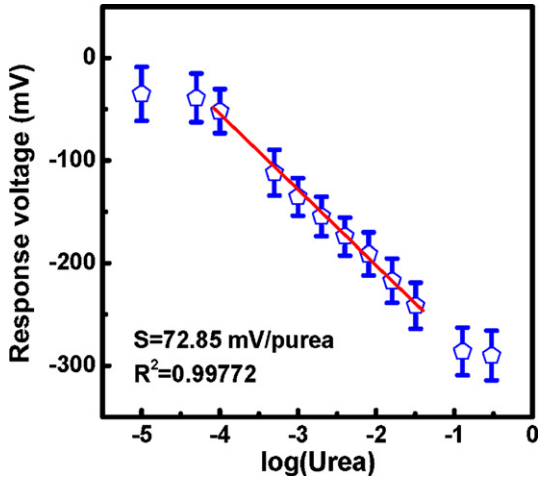

Fig. 8. Response voltage of the urea biosensor based on pH-sensitive EIS devices incorporating a Sm_2TiO_5 sensing film (RTA at 900 °C) plotted as a function of the urea concentration.

4. Conclusions

We have developed high-performance EIS devices incorporating thin Sm_2TiO_5 sensing membranes grown on Si substrates by reactive co-sputtering. We used XRD AES, and AFM to confirm the presence of the Sm_2TiO_5 structures in these EIS devices. Thin Sm_2TiO_5 EIS device that we had subjected to RTA at 900 °C exhibited an optimum pH sensing performance including a higher sensitivity of 60.5 mV/pH, a smaller hysteresis voltage of 2.72 mV and a lower drift rate of 1.15 mV h^{-1}. The selectivity coefficients of Sm_2TiO_5 sensors for ion Na^+, K^+, Ca^{2+}, and Mg^{2+} are at −5.94, −5.66, −6.52, and −6.56, respectively. This improvement is attributed to the lower number of crystal defects and the higher surface roughness occurred at this condition. Furthermore, a urea biosensor based on pH-sensitive Sm_2TiO_5 EIS device exhibited a sensitivity towards the detection of urea of 72.85 mV/purea.

Acknowledgment

This work was supported by the National Science Council, Taiwan, Republic of China, under contract no. NSC-98-2221-E-182-056-MY3.

References

[1] P. Bergveld, IEEE Trans. Biomed. Eng. 17 (1970) 70.
[2] Y.L. Chin, J.C. Chou, T.P. Sun, H.K. Liao, W.Y. Chung, S.K. Hsiung, Sens. Actuators B 75 (2001) 36.
[3] L. Bousse, H.H. van den Vlekkert, N.F. de Rooij, Sens. Actuators B 2 (1990) 103.
[4] L. Bousse, S. Mostarshed, B. van der Schoot, N.F. de Rooij, Sens. Actuators B 17 (1994) 157.
[5] A. Fog, R.P. Buck, Sens. Actuators 5 (1984) 137.
[6] C.N. Tsai, J.C. Chou, T.P. Sun, S.K. Hsiung, Sens. Actuators B 108 (2005) 877.
[7] J.C. Chou, J.L. Chiang, Sens. Actuators B 66 (2000) 106.
[8] S. Yoshida, N. Hara, K. Sugimoto, J. Electrochem. Soc. 151 (2004) H53.
[9] C.S. Lai, C.M. Yang, T.F. Lu, Electrochem. Solid-State Lett. 9 (2006) G90.
[10] T.M. Pan, K.M. Liao, Sens. Actuators B 128 (2007) 245.
[11] T.M. Pan, K.M. Liao, Sens. Actuators B 133 (2008) 97.
[12] L.B. Chang, H.H. Ko, Y.L. Lee, C.S. Lai, C.Y. Wang, J. Electrochem. Soc. 153 (2006) G330.
[13] T.M. Pan, J.C. Lin, M.H. Wu, C.S. Lai, Sens. Actuators B 138 (2009) 619.
[14] Y.S. Lin, R. Puthenkovilakam, J.P. Chang, Appl. Phys. Lett. 81 (2002) 2041.
[15] H. Yang, H. Wang, H.M. Luo, D.M. Feldmann, P.C. Dowden, R.F. DePaula, Q.X. Jia, Appl. Phys. Lett. 92 (2008) 062905.
[16] T.M. Pan, C.C. Huang, Electrochem. Solid-State Lett. 11 (2008) G62.
[17] T. Schroeder, G. Lupina, J. Dabrowski, A. Mane, Ch. Wenger, G. Lippert, H.J. Mussig, Appl. Phys. Lett. 87 (2005) 022902.
[18] C.H. Liu, T.M. Pan, W.H. Shu, K.C. Huang, Electrochem. Solid-State Lett. 10 (2007) G54.
[19] S. Jeon, H. Hwang, Appl. Phys. Lett. 81 (2002) 4856.

[20] L. Miotti, K.P. Bastos, C. Driemeier, V. Edon, M.C. Hugon, B. Agius, I.J.R. Baumvol, Appl. Phys. Lett. 87 (2005) 022901.
[21] C.D. Fung, P.W. Cheung, W.H. Ko, IEEE Trans. Electron Devices 33 (1986) 8.
[22] L. Bousse, N.F. de Rooij, P. Bergveld, IEEE Trans. Electron Devices 30 (1983) 1263.
[23] R.E.G. van Hal, J.C.T. Eijkel, P. Bergveld, Sens. Actuators B 24 (1995) 201.
[24] W. Torbicz, Z. Sypniewska, Sens. Actuators B 7 (1992) 565.
[25] E.H. Nicollian, J.R. Brews, MOS Physics and Technology, Wiley, New York, 1982.
[26] M.V. Fischetti, S.E. Laux, J. Appl. Phys. 89 (2001) 1205.
[27] H. Scher, E.W. Montroll, Phys. Rev. B 12 (1975) 2455.
[28] G. Pfister, H. Scher, Phys. Rev. B 15 (1977) 2062.
[29] J. Kakalios, R.A. Street, W.B. Jackson, Phys. Rev. Lett. 59 (1987) 1037.
[30] E. Bakker, E. Pretsch, P. Bhlmann, W.B. Jackson, Anal. Chem. 72 (2000) 11273.
[31] T. Matsuo, M. Esashi, H. Abe, IEEE Trans. Electron Devices 26 (1979) 1856.
[32] M.J. Schoning, Y.G. Mourzina, J. Schubert, W. Zander, A. Legin, Y.G. Vlasov, H. Luth, Sens. Actuators B 78 (2001) 273.
[33] J.L. Chiang, S.S. Jan, J.C. Chou, Y.C. Chen, Sens. Actuators B 76 (2001) 624.
[34] P.D. Kirsch, C.S. Kang, J. Lozano, J.C. Lee, J.G. Ekerdt, J. Appl. Phys. 91 (2002) 4353.
[35] H. Barhoumi, A. Maaref, M. Rammah, C. Martelet, N. Jaffrezic, C. Mousty, S. Vial, C. Forano, Mater. Sci. Eng. C 26 (2006) 328.
[36] N.H. Chou, J.C. Chou, T.P. Sun, S.K. Hsiung, IEEE Sens. J. 6 (2006) 262.
[37] A. Maaref, H. Barhoumi, M. Rammah, C. Martelet, N. Jaffrezic-Renault, C. Mousty, S. Cosnier, Sens. Actuators B 123 (2007) 671.
[38] M. Singh, N. Verma, A.K. Garg, N. Redhu, Sens. Actuators B 134 (2008) 345.
[39] G. Dhawan, G. Sumana, B.D. Malhotra, Biochem. Eng. J. 44 (2009) 42.